A Family of Vernier Permanent Magnet Machines Utilizing An Alternating Rotor Leakage Flux Blocking Design

Wenbo Liu
Department of Electrical and Computer Engineering
University of Wisconsin
Madison WI, USA
Wliu86@wisc.edu

Thomas A. Lipo
Department of Electrical and Computer Engineering
University of Wisconsin
Madison WI, USA
lipo@engr.wisc.edu

***Abstract*—Since the vernier machine (VM) is a flux modulation machine that also operates simultaneously as a synchronous machine, the torque producing mechanism of this device is difficult to understand. This paper begins with an analytical study of a synchronous permanent magnet (PM) machine, where the back-emf and torque are derived based on a generic number of slots per pole per phase stator. Numerical comparison of these two quantities is then made between an interior permanent magnet (IPM) machine and a vernier permanent magnet (VPM) machine. Performance predictions and design observations of the VPM are obtained. A new topology for a single air gap spoke type vernier permanent magnet (SVPM) machine using ferrite magnets is then proposed, where alternating flux barriers are placed at the bottom of pair-wise magnets on the rotor. Alternative topologies that share the same principle with V-shape and U-shape rare earth magnets are also introduced. Overall, the improved spoke type SVPM design effectively boosts the back-emf induction compared to the conventional SVPM, and torque production even surpasses that of a benchmark rare earth IPM machine although with a slightly lower power factor. However, if one adopts the V-/U-shape rare earth magnet design, it is shown that an 80% torque improvement and comparable power factor can be obtained. These results draw the conclusion that the new alternating rotor leakage flux blocking topology shows considerable promise in low and medium speed applications both as a motor or generator.**

Keywords—vernier machine; spoke type; ferrite magnet; alternating flux barrier; alternating rotor leakage flux blocking; low speed; high torque density

NOMENCLATURE

θ_s	Spatial angle of the stator MMF.
θ_r	Spatial angle of the rotor magnet.
θ_{rm}	Mechanical rotor rotation angle.
k_{wh}	h[th] harmonic winding factor.
N_s, N_t	Turns per phase, total number of turns.
I_{pk}	Stator peak current.
C_p	Number of parallel circuits.
P_s, P_r	Number of stator poles, and number of rotor poles.
S_s	Number of stator slots.
γ	Current phase shift angle.
γ_0	Stator slot pitch angle.
$\hat{p}_0$, $\hat{p}_h$	dc and h[th] harmonic component of relative permeance
B_{gap}	Air gap flux density.
H_{gap}	Air gap magnetic field intensity.
V_{gap}	Volume of the air gap.
l_{stk}	Stack length.
r	Stator inner radius

I. INTRODUCTION

Many industries require machines to either produce high torque at low speed such as industrial cooling fans, or vice visa, to convert power from a low-speed high-torque prime mover back to electricity such as a wind turbine. The power level of these applications can range from kW to multi-MW, and since the system using VMs can be simplified to operate as a direct drive configuration without gearbox, the VM drive may require less maintenance time and cost. However, the VM is a flux modulation machine whose mechanism is yet difficult to understand. Considerable effort has been directed to the analytical analysis when the VM was first introduced as a synchronous reluctance machine variant [1], and then extended to the permanent magnet version [2],[3]. An analytical form of back-emf induction and torque production were derived in [4],[5] for a surface mount PM topology and in [6],[7] for a spoke type PM topology. However, no explicit analysis for a generic stator considering magnet usage has yet been reported.

The purpose of this paper is twofold. First, an analytical study of a synchronous PM machine is presented, which has a generic stator with q number of stator slots per pole per phase. Given the same amount of magnet usage, a performance comparison including back-emf induction and torque production are made between interior permanent magnet (IPM) machines and vernier permanent magnet machines (VPM). Second, a novel spoke type vernier permanent magnet machine (SVPM), which uses ferrite magnets with an alternating flux barrier design is proposed. Alternative topologies that share the same principle with V-shape and U-shape rare earth magnets are also introduced. All three new

978-1-5090-2998-3/17/$31.00 ©2017 IEEE

topologies can be categorized as a new family of VPMs that utilize alternating rotor leakage flux blocking effects. Key results are benchmarked against a conventional ferrite SVPM and with an existing low-speed commercially available IPM using rare earth magnets.

II. Analysis of Operating Principle

The VPMs can be considered as a type of synchronous machine where the rotor field rotates only at a definite fraction of the angular speed of the stator rotating field. This rotor mechanical speed is relatively slow as the result of an electric gear down effect, which in turn, helps boost the torque production. However, electrically, the rotor field must still be synchronized with stator field in the same manner as a normal synchronous machine. This section begins with machine fundamentals, devoting effort to a more generic and detailed analytical analysis of PM type synchronous machine back-emf induction and torque production with the aim to further understand the mechanism of VPMs, and differentiate this category from normal PM synchronous machines. The investigation focuses on factors such as: number of slot per pole per phase (q), stator slot pitch (τ_s), slot opening (b_0), airgap length (g), and magnet usage which have not yet been systematically reported in the literature. Innovations and observations are proposed and included as well.

To initiate the derivation of magnet induced back-emf, the angular references axes of stator, rotor, and rotor rotation are shown in Fig. 1, in which the counter-clockwise direction indicates a positive angle rotation. The relation of the three angles at an arbitrary position can be described as

$$\theta_r = \theta_s - \theta_{rm} \tag{1}$$

Three generic models, corresponding to a conventional SVPM, a proposed SVPM, and an IPM are shown from left to right in Fig.1. The three machines share a same generic stator, where the back-emf seen in stator winding can be expressed as the rate of change of no load flux linkages over time as

$$e = \frac{d\lambda}{dt} = \frac{d\lambda}{d\theta_{rm}}\frac{d\theta_{rm}}{dt} = \omega_{rm}\frac{d\lambda}{d\theta_{rm}} \tag{2}$$

where $d\lambda = rl_{stk}N(\theta_s)B_{rg}(\theta_s,\theta_{rm})d\theta_s$ .One must first eliminate θ_s to obtain an explicit form of back-emf. This can be done by integrating the $d\lambda$ over one stator pole pitch as

$$\lambda = \int_0^{2pi/P_s} d\lambda = rl_{stk}\int_0^{2pi/P_s} N(\theta_s)B_{rg}(\theta_s,\theta_{rm})d\theta_s \tag{3}$$

where the winding function $N(\theta_s)$ and magnet induced airgap flux density $B_{rg}(\theta_s,\theta_{rm})$ are the key components needed to obtain the per phase flux linkages. More specifically, $N(\theta_s)$ is related to the stator slot configuration: q, and $B_{rg}(\theta_s,\theta_{rm})$ is determined by both the rotor magnet usage and stator slot geometry (i.e. τ_s, b_0, g).

Assuming here that the stator only has one winding layer, resulting in a 60 degree phase belt as shown in Fig. 2. A stepwise winding function with an arbitrary q number can be represented by a Fourier series. The generic form for $N(\theta_s)$ with respect to P_s stator poles and q can be written as

$$N(\theta_s) = \frac{4}{\pi}N_s\sum_{h=1,3,5\ldots}\frac{k_{wh}}{h}\cos\left(h\frac{P_s}{2}\theta_s\right) \tag{4}$$

where the winding factor k_{wh} is a function of q. If q = 1,

$$k_{wh} = \sin\left(\frac{h\pi}{2}\right) \tag{5}$$

If q is even,

$$k_{wh} = \frac{2\sin(hq\gamma_0/4)\sin\left(h(2\pi - q\gamma_0)/4\right)}{q\sin(h\gamma_0/2)} \tag{6}$$

If q is odd and larger than 1,

$$k_{wh} = \frac{-\cos(h\pi/2)\cos(h\gamma_0/2) - \cos\left(h(\pi - q\gamma_0)/2\right)}{q\sin(h\gamma_0/2)} \tag{7}$$

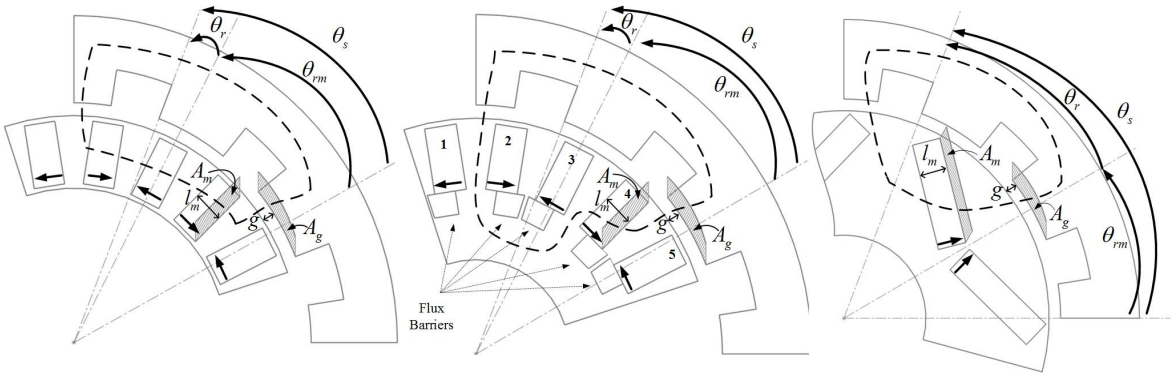

(a) Conventional SVPM. (b) Proposed SVPM (c) IPM

Fig. 1. Model demonstration and topologies comparison between SVPM and IPM

It should be noted that the winding factor is determined by the choice of q. For q larger than unity, there is a slot pitch angle γ_0 introduced (assuming a full pitch winding configuration). The corresponding k_{wh} values for the first 6 harmonics are tabulated in Table. I, which will be incorporated into the back-emf calculation later.

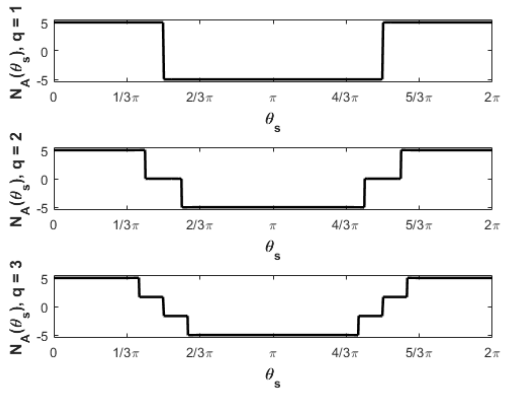

Fig. 2. Winding function with a 60 degree phase belt

TABLE I. WINDING FACTOR COEFFICIENT

k_w	$q = 1$	$q = 2$	$q = 3$	$q = 4$
1st	1.00	0.97	0.96	0.96
3rd	-1.00	-0.71	-0.67	0.65
5th	1.00	0.26	0.22	0.21
7th	-1.00	0.26	0.18	0.16
9th	1.00	-0.71	-0.33	0.27
11th	-1.00	0.97	0.18	0.13

In a PM synchronous machine, magnet induced airgap flux density $B_{rg}(\theta_s,\theta_{rm})$ can be viewed as the magnet airgap flux density B_g in ideal smooth/slotless airgap modulated by the stator teeth, where the relative permeance $\hat{p}$ is included to account for the permeance variation along the stator inner surface as

$$B_{rg}(\theta_s,\theta_{rm}) = \hat{p}(\theta_s) B_g(\theta_r) \tag{8}$$

The relative permeance and ideal airgap flux density can be readily expressed in the form of Fourier series as

$$\hat{p}(\theta_s) = \hat{p}_0 + \sum_{h=1,3,5\ldots} \hat{p}_h \cos(hS_s\theta_s) \tag{9}$$

$$B_g(\theta_r) = \sum_{h=1,3,5\ldots} B_{gh} \cos\left(\frac{P_r}{2}\theta_r\right) \tag{10}$$

The relative permeance here is unitless, determined by stator slot geometry (i.e. τ_s, b_0, g), and operates in a manner similar to Carter's coefficient. If one considers the fundamental and dc (if there is any) components of (9) and (10), these two components have the largest magnitude and are the most effective in producing airgap flux. By incorporating (1), (9), (10) to (8), the airgap flux density can be expressed as

$$\begin{aligned} B_{rg}(\theta_s,\theta_{rm}) &= B_{g1}\cos\left(\frac{P_r}{2}(\theta_s-\theta_{rm})\right)\left[\hat{p}_0+\hat{p}_1\cos(S_s\theta_s)\right] \\ &= B_{g1}\left[\frac{1}{2}\hat{p}_1\cos\left(\left(\frac{P_r}{2}-S_s\right)\theta_s-\frac{P_r}{2}\theta_{rm}\right)+\hat{p}_0\cos\left(\frac{P_r}{2}(\theta_s-\theta_{rm})\right)+\right. \\ &\qquad \left.\frac{1}{2}\hat{p}_1\cos\left(\left(\frac{P_r}{2}+S_s\right)\theta_s-\frac{P_r}{2}\theta_{rm}\right)\right] \end{aligned} \tag{11}$$

In (11), B_{g1} is the only quantity left to be related to the machine physical parameters before proceeding to the derivation of back-emf, which shall be seen as important as related to magnet usage. If one assumes a certain amount usage of magnet in synchronous PM machine design, for given stack length, and same magnet thickness (same sustainability to fault current), the total magnet surface area is a fixed value: A_{mT}. Given the slot and pole number combination for the SVPMs as

$$\pm P_s = P_r - 2S_s \tag{12}$$

where, the stator slots can be written as

$$S_s = 3P_s q \tag{13}$$

A_{mT} can be related to the magnet surface area for each magnet bar in Fig. 1 for SVPM and IPM respectively as

$$A_{mT} = (6q \pm 1) \times P_s A_{m\_SVPM} \tag{14}$$

$$A_{mT} = 2 \times P_s A_{m\_IPM} \tag{15}$$

Equation (14) is also true for a surface mount magnet type VPM. The ratio of VPM bar magnet surface area over that of an IPM is then

$$A_{m\_SVPM} / A_{m\_IPM} = 2/(6q \pm 1) \tag{16}$$

Assuming ideal iron core material and no leakage flux, the flux density in the magnet bar in a conventional SVPM and an IPM can be expressed by the load line respectively as

$$B_{m\_SVPM} = -\mu_0 \left(\frac{A_g}{A_{m\_SVPM}}\right)\left(\frac{l_m}{g + n_c l_m}\right) H_m \tag{17}$$

$$B_{m\_IPM} = -\mu_0 \left(\frac{A_g}{A_{m\_IPM}}\right)\left(\frac{l_m}{g}\right) H_m \tag{18}$$

By comparing (17) and (18), one can find that the flux density in the magnet bar of a conventional SVPM is smaller than the IPM ($B_{m\_SVPM}/B_{m\_IPM}<1$), due to the presence of magnets in the flux path, which adds an extra equivalent airgap length as shown in Fig. 1(a). However, an IPM design does not have such issues as shown in Fig. 1(c). As a result, the flux density for the two machines in the air gap per phase can be written as

$$B_{g\_SVPM}=\left(\frac{A_{mT}/P_s}{A_g}\right)B_{m\_SVPM}=\frac{\pi}{4}B_{g1\_SVPM} \tag{19}$$

$$B_{g\_IPM}=\left(\frac{A_{mT}/P_s}{A_g}\right)B_{m\_IPM}=\frac{\pi}{4}B_{g1\_IPM} \tag{20}$$

This result suggests that the ratio $B_{g1\_SVPM}/B_{g1\_IPM}<1$. Here, an ideal assumption is made that all the magnet flux in the SVPM (or IPM) per stator pole is linked to the stator coils, whereas the SVPM tends to have less flux linkage in actual case, indicating the air gap flux density ratio between a conventional SVPM and an IPM might be even smaller.

To impove this ratio, an alternating flux barrier design on the rotor is proposed, with the aim of reducing the airgap length in (17) as shown in Fig. 1(b). As the new flux path is enabled in the proposed design, fewer magnets that act as the airgap need to be traversed to enclose a flux path, thus the flux density in the magnet bar in the proposed SVPM is:

$$B_{g\_SVPM}^{proposed}=-\mu_0\left(\frac{A_g}{A_{m\_SVPM}}\right)\left(\frac{l_m}{g+n_p l_m}\right)H_m \tag{21}$$

where $0<n_p<n_c$, leading to

$$B_{g\_SVPM}<B_{g\_SVPM}^{proposed}<B_{g\_IPM} \tag{22}$$

equivalently in the form of the fundamental component:

$$B_{g1\_SVPM}<B_{g1\_SVPM}^{proposed}<B_{g1\_IPM} \tag{23}$$

Now one can draw the conclusion that, with the same magnet usage, both conventional and proposed SVPM has smaller airgap flux density compared with IPM machine, due to the presence of the extra equivalent airgap length on the no load flux path.

By incorporating (3), (4), (11), (12), (13) to (2), the back-emf for SVPMs can be expressed as

$$e_{SVPM}=\left(\frac{k_1}{1}\hat{p}_1+\frac{2k_{6q\pm1}}{6q\pm1}\hat{p}_0+\frac{k_{12q\pm1}}{12q\pm1}\hat{p}_1\right)\times rl_{stk}N_sB_{g1\_VPM}\omega_{rm}\frac{P_r^{SVPM}}{P_s}\sin\left(\frac{P_r^{SVPM}}{2}\theta_{rm}\right) \tag{24}$$

where $P_r^{SVPM}=(6q\pm1)P_s$. On the other hand, the back-emf for an IPM can be expressed as

$$e_{IPM}=\left(\frac{k_{|1-6q|}}{|1-6q|}\hat{p}_1+\frac{2k_1}{1}\hat{p}_0+\frac{k_{1+6q}}{1+6q}\hat{p}_1\right)\times rl_{stk}N_sB_{g1\_IPM}\omega_{rm}\frac{P_r^{IPM}}{P_s}\sin\left(\frac{P_r^{IPM}}{2}\theta_{rm}\right) \tag{25}$$

where $P_r^{IPM}=P_s$. A magnitude ratio of back-emf between SVPMs and IPMs can be easily found as

$$\frac{e_{SVPM}}{e_{IPM}}=\frac{B_{g1\_SVPM}}{B_{g1\_IPM}}\frac{(6q\pm1)}{1}\frac{K_{SVPM}}{K_{IPM}} \tag{26}$$

where the ratio of harmonic components is

$$\frac{K_{SVPM}}{K_{IPM}}=\frac{\frac{k_1}{1}\hat{p}_1+\frac{2k_{6q\pm1}}{6q\pm1}\hat{p}_0+\frac{k_{12q\pm1}}{12q\pm1}\hat{p}_1}{\frac{k_{|1-6q|}}{|1-6q|}\hat{p}_1+\frac{2k_1}{1}\hat{p}_0+\frac{k_{1+6q}}{1+6q}\hat{p}_1} \tag{27}$$

As mentioned above, the relative permeance is determined by stator slot geometry (i.e. τ_s, b_0, g). More specifically, the relative permeance is the function of these geometries as

$$\hat{p}_1=\hat{p}_1(b_0/\tau_s,b_0/g),\hat{p}_0=\hat{p}_0(b_0/\tau_s,b_0/g) \tag{28}$$

The details are given in [8]. Thus, for a specific design, the relative permeance can be calculated with given parameters as shown in Fig. 3. The results suggest that: $\hat{p}_0$ is largest and $\hat{p}_1$ is smallest with smooth/slotless stator when b_0/g is 0, corresponding to no permeance variation. The difference between $\hat{p}_0$ and $\hat{p}_1$ starts to decrease as b_0/g and b_0/τ_s increases, corresponding to a progressively larger permeance variation in the airgap. For a given size machine, the value of b_0/g depends on the choice of q, for small q number, b_0/g tends to have a value usually greater than 15, since the slot opening is larger. However, for a larger q number, b_0/g falls into a smaller range of values.

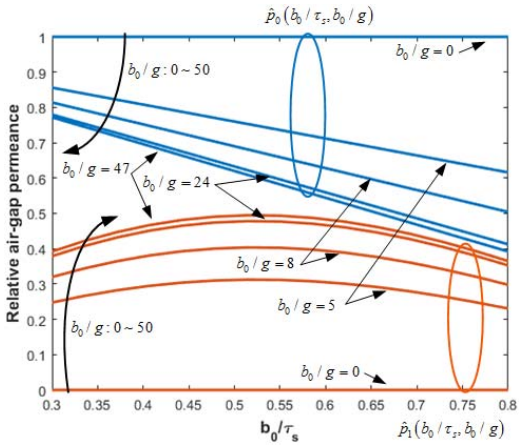

Fig. 3. Fundamental and dc component of relative permeance

With all of the geometry parameters specified, a numerical comparison of emf can be obtained from (26) as:

$$\frac{e_{SVPM}}{e_{IPM}}=\frac{B_{g1\_SVPM}}{B_{g1\_IPM}}\frac{(6q\pm1)}{1}\frac{K_{SVPM}}{K_{IPM}}<\frac{(6q\pm1)}{1}\frac{K_{SVPM}}{K_{IPM}} \tag{29}$$

where the ratios of harmonic components are plotted in Fig. 4. The results indicate that, given the stator configuration, a SVPM design with $P_r^{SVPM}=(6q-1)P_s$ will generate larger harmonic components (or back-emf) compared with the alternative case of $P_r^{SVPM}=(6q+1)P_s$. It is preferred to use the value of q=1 and a value of $b_0/\tau_s>0.5$ to maximize the back-

emf induction. The reason behind is that, according to Fig. 5, the harmonic component of SVPM with $P_r^{SVPM}=(6q-1)P_s$ tends to have a larger value following the expression in (24) as q decreases. On the other hand, the remaining two harmonic components show less sensitivity to variation in q. Therefore, for the ideal case, the largest back-emf ratio between SVPM ($P_r^{SVPM}=(6q\pm1)P_s$) and IPM is obtained when q=1:

$$\frac{e_{SVPM}}{e_{IPM}}=\frac{B_{g1\_SVPM}}{B_{g1\_IPM}}\frac{(6q-1)}{1}\frac{K_{SVPM}}{K_{IPM}}<\frac{(6q-1)}{1}\frac{K_{SVPM}}{K_{IPM}}<0.6\times5=3 \tag{30}$$

$$\frac{e_{SVPM}}{e_{IPM}}=\frac{B_{g1\_SVPM}}{B_{g1\_IPM}}\frac{(6q+1)}{1}\frac{K_{SVPM}}{K_{IPM}}<\frac{(6q+1)}{1}\frac{K_{SVPM}}{K_{IPM}}<0.3\times7=2.1 \tag{31}$$

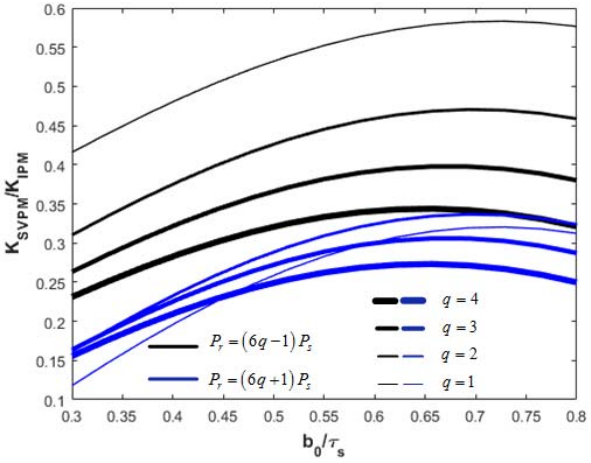

Fig. 4. Ratio of harmonic components between SVPM and IPM

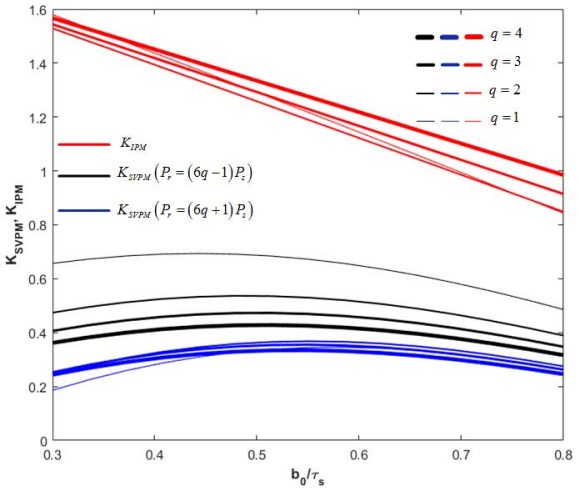

Fig. 5. Harmonic components of SVPM and IPM

The torque will be calculated in a similar manner as is back-emf. The torque can be expressed as

$$T=\frac{\partial}{\partial\theta_{rm}}\left[\int_{V_{gap}}B_{gap}H_{gap}dV_{gap}\right]\approx\frac{d_{is}l_i}{2}\int_0^{2\pi}\left(\frac{\partial}{\partial\theta_{rm}}B_{rg}\right)F_{sg}d\theta_s \tag{32}$$

where, B_{rg} has already been found in (11). The stator MMF is derived in [9] as

$$F_{sg}=\sum_{h=1,5,7,11\ldots}\left(\frac{3}{2\pi}\right)\frac{k_hN_tI_{pk}}{hC_pP_s}\cos\left(h\frac{P_s}{2}\theta_s\pm(\omega_et-\gamma)\right) \tag{33}$$

where the - sign is picked for h = 1,7,13…, representing a counter-clockwise rotating wave, + sign is picked for h = 5,11,17…, representing a clockwise rotating wave. The cosine term in (33) share the same spatial frequency as the winding function in (4). Thus, the integration over stator inner surface in (32) will result in a similar form as in (24), (25). The torque for SVPMs can be expressed as

$$T_{SVPM}=\left(\frac{k_1}{1}\hat{p}_1+\frac{2k_{6q\pm1}}{6q\pm1}\hat{p}_0+\frac{k_{12q\pm1}}{12q\pm1}\hat{p}_1\right)\times \frac{3N_tI_{pk}B_{g1\_VPM}}{2C_p}\frac{P_r^{SVPM}}{P_s}\sin\left(\gamma+\frac{P_r^{SVPM}}{2}\theta_{rm}\mp\omega_et\right) \tag{34}$$

It should be noted that the + sign is obtained in the sine term of (34) corresponding to the case $P_r^{SVPM}=(6q-1)P_s$, which means the rotor rotates in the clockwise direction that is opposite to the MMF. The torque for IPM can be expressed as

$$T_{IPM}=\left(\frac{k_{|1-6q|}}{|1-6q|}\hat{p}_1+\frac{2k_1}{1}\hat{p}_0+\frac{k_{1+6q}}{1+6q}\hat{p}_1\right)\times \frac{3N_tI_{pk}B_{g1\_IPM}}{2C_p}\frac{P_r^{IPM}}{P_s}\sin\left(\gamma+\frac{P_r^{IPM}}{2}\theta_{rm}-\omega_et\right) \tag{35}$$

Therefore, a torque ratio for MTPA can also be obtained as

$$\frac{T_{SVPM}}{T_{IPM}}=\frac{B_{g1\_SVPM}}{B_{g1\_IPM}}\frac{(6q\pm1)}{1}\frac{K_{SVPM}}{K_{IPM}} \tag{36}$$

The ratio of harmonic components, K_{SVPM}/K_{IPM} has been defined in (27). Thus, similar conclusions can be reached. For the ideal case, the largest torque ratio between the SVPM where $P_r^{SVPM}=(6q\pm1)P_s$ and an IPM is obtained when q=1

$$\frac{T_{SVPM}}{T_{IPM}}<\frac{(6q-1)}{1}\frac{K_{SVPM}}{K_{IPM}}<0.6\times5=3 \tag{37}$$

$$\frac{T_{SVPM}}{T_{IPM}}<\frac{(6q+1)}{1}\frac{K_{SVPM}}{K_{IPM}}<0.3\times7=2.1 \tag{38}$$

Thus far, it has been found that the torque production of synchronous PM machine is proportional to the back-emf induction, for a given stator and magnet usage. It is preferred to adopt an SVPM design, more specifically: the design with $P_r^{SVPM}=(6q-1)P_s$, which reaches ideally 3 times the output torque of an IPM design at the expense of a higher terminal voltage as demonstrated in Fig. 6. The terminal voltage V_{IPM} of the IPM machine can be found for a given synchronous reactance X_s. The terminal voltage of the SVPM with the same stator and magnet usage tends to be larger, and corresponds to poorer power factor (larger power factor angle). This result is because the reactance of SVPM becomes scaled up by a factor of 6q-1, while the back-emf only becomes boosted by only a

fraction of $6q$-1, namely $K_{SVPM}/K_{IPM,}$ whose value can be up to 0.6. Thus, based on the analytical analysis with some ideal assumptions, the SVPM machine can produce more torque than an IPM machine with the same copper loss and magnet usage. On the other hand, the iron loss could be higher due to higher excitation frequency, and a larger power rated drive is obviously required to achieve the torque capability of the improved machine.

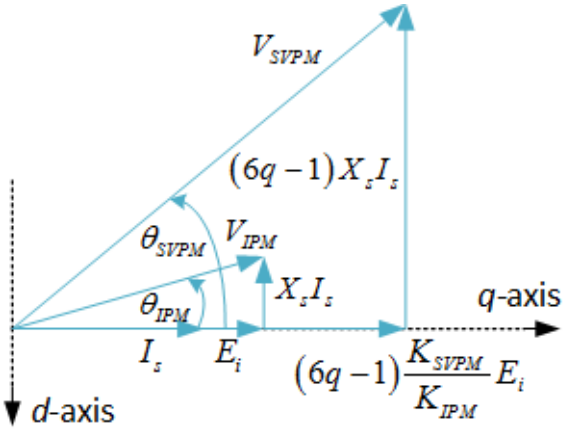

Fig. 6. Phasor diagram of SVPM and IPM

III. Alternating Rotor Leakage Flux Blocking Design

This section introduces an alternating flux barrier design on the rotor of an SVPM in which the spoke type structure is considered to be ideal for the adoption of cost-effective ferrite magnets. A proposed and a conventional SVPM design using ferrite magnets are first compared, then U-/V- shape topologies using rare earth magnets that share the same principle of the alternating rotor leakage flux blocking structure are also proposed. Finally, the three new designs are benchmarked against a commercially available IPM using rare earth magnets for an industrial cooling fan application.

A. Alternating flux barrier design on SVPM

Following the derivations of the previous section, A 4 stator pole, 20 rotor pole SVPM of the conventional topology and the proposed topology are shown in Fig. 8. For the conventional topology, as a zoomed-in rotor view in Fig. 8(a) suggests the rotor radial space is mostly occupied by the ferrite magnets with thin iron bridges on the top and bottom to hold the magnets in place. For the proposed design in Fig. 8(d), an alternating flux barrier structure is placed on the bottom of pair-wise spoke type magnets, where the key design parameters are delineated. The barriers need to be of low permeability material, which are connected by a thin iron bridge. The iron bridge can help limit axial leakage flux at the rotor ends and eliminate any unbalanced force [10]. The corresponding no load flux line distributions are shown in Fig. 8(b), and (e), where the flux from rotor magnets that links to the coil set A can be extracted by simple inspection. Two major rotor magnet flux paths specified in red and orange, that links coil A in the conventional SVPM design can be observed in Fig. 8(b), with colored arrows indicating the corresponding flux direction. By adopting the proposed design, there are three major rotor magnet flux paths, linking four magnets to coil A. The extra iron space created in between pair-wise adjacent magnets is also a part of the flux path colored in brown and helps include two additional magnets to link coil A. It also should be noted that the alternating use of rotor flux barriers allows the use of an enlarged rotor back iron without producing a magnetic short circuit of the rotor magnets. This result is verified by the emf plots in Fig. 8(c), and (f), where the fundamental of phase voltage becomes doubled with the simple modification on the rotor, and the voltage waveform also becomes more sinusoidal.

In general, the proposed alternating flux barrier structure appears to produce reluctance variations on the rotor, which might cause a saliency difference such as an IPM machine. A study of the flux linkage at different rotor position is presented in Fig. 7. The results, however, show that the fluctuations of flux linkage vs. rotor position is very limited, i.e. within 10%. Thus, the proposed machine such as the one in Fig. 6 need to be modeled only as an SPM with no saliency.

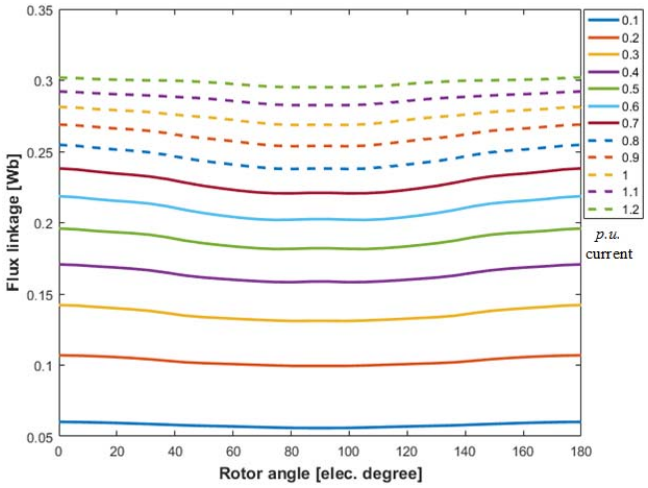

Fig. 7. Flux linkage at different rotor positions with changes in current

B. Alternative topologies using rare earth magnets

It is also possible to replace the ferrite magnets following the same principle for the proposed SVPM design. However, the pair-wise rare earth magnets would tend to demagnetize each other at its bottom portion due to the limited distance between them. The alternative design is to replace the spoke type magnet with V-shape magnet sitting on a pair of flux barriers as demonstrated in Fig. 9(a), where the rotor pole pitch is spaced evenly for N and S poles. However, variations might be applied to the ratio of pole pitch between N and S pole to obtain design objectives such as maximizing torque production or torque ripple minimization. Another topology is to adopt U-shape magnet, where one horizontal bar magnet is placed between two short radial magnets, with flux barriers in placed to limit leakage flux as shown in Fig. 9(b). Thus, some space can be saved on the rotor back iron portion which will help reduce the rotor inertia. The two topologies function in

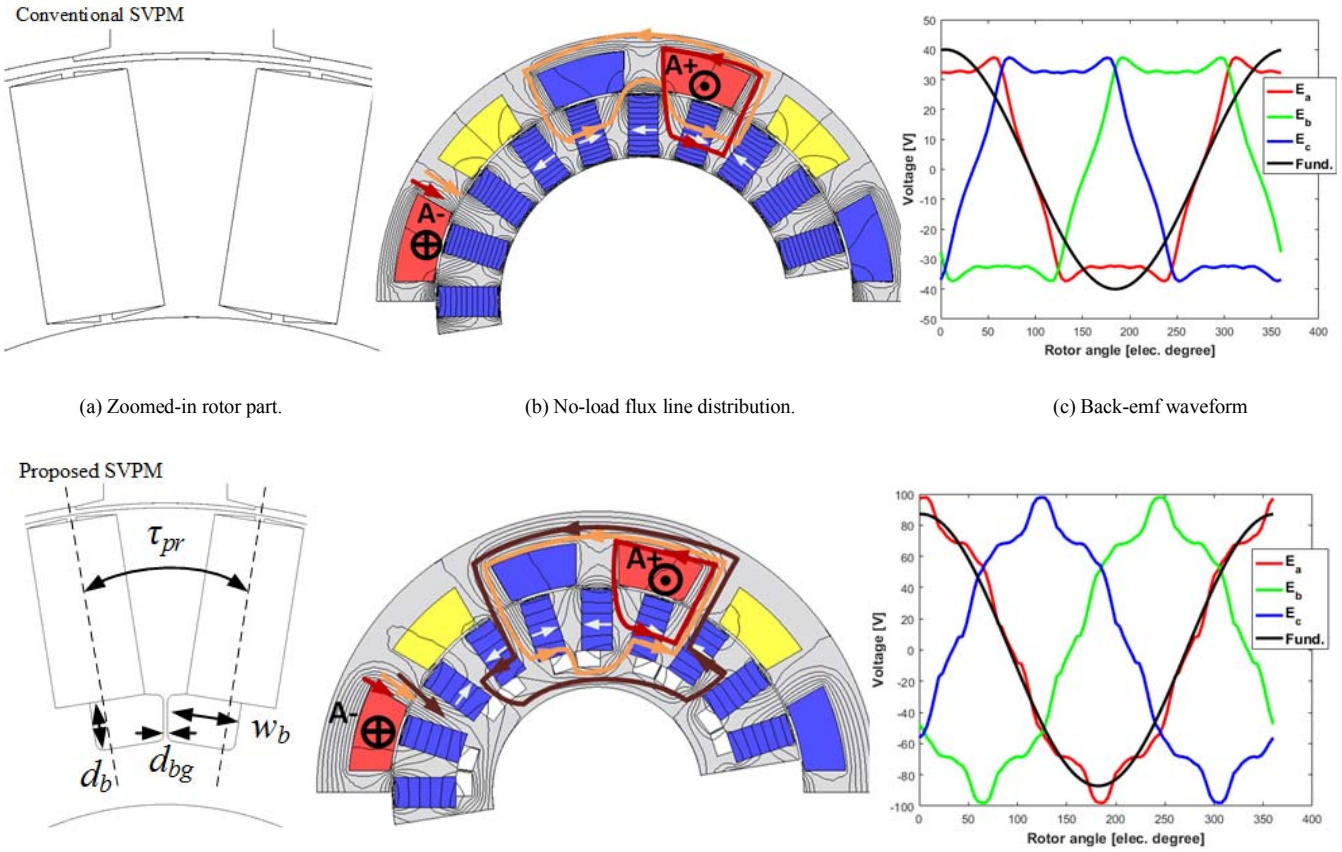

(a) Zoomed-in rotor part. (b) No-load flux line distribution. (c) Back-emf waveform

(d) Zoomed-in rotor part. (e) No-load flux line distribution. (f) Back-emf waveform

Fig. 8. Conventional design and alternating flux barrier design with no-load study

the same manner as the alternating flux barrier design in SVPM. In general, these three new topologies can be considered to be a new family of VPMs that utilize alternating rotor leakage flux blocking techniques. Multi-layer magnet topology using V-shape/U-shape magnet is also possible, but are yet to be explored.

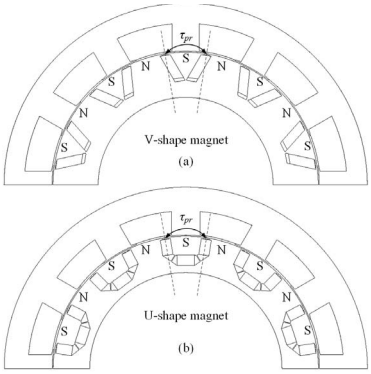

Fig. 9. Alternative topologies using rare earth magnets

C. *Topology design comparison*

The proposed SVPM using ferrite magnets and V-/U-shape VPM using rare earth magnets have been designed, following the discussion in the previous section for an industrial cooling fan application. To make a fair comparison between conventional SVPM, the proposed topologies and an existing, commercially available benchmark IPM by a major motor manufacturer. The machine outer stator diameter and stack length are kept the same, as well as the stator current density. A comparison of key parameters and performance quantities are tabulated in Table II. The results show that the proposed SVPM and V-/U- shape VPMs outperform the benchmark IPM in torque production. The proposed SVPM needs to use about twice the weight of ferrite magnets with a somewhat lower power factor due to the small remanence of the ferrite. The V-/U- shape VPM improves the torque by about 80% using the same amount of magnet, and achieves a similar power factor compared with benchmark machine. Meanwhile, only minimum modifications were made to the rotor to achieve the degree of performance improvement obtained.

TABLE II KEY PARAMETERS AND PERFORMANCE COMPARISON

	Benchmark motor	Conventional SVPM	Proposed SVPM	V-shape VPM	U-shape VPM
Machine type	IPM	VPM	VPM	VPM	VPM
Magnet type/B_r [T]	NdFeB/1.2	Ferrite/0.42	NdFeB/1.2	NdFeB/1.2	NdFeB/1.2
Stator/rotor pole number	4/4	4/20	4/20	4/20	4/20
SPP	4	1	1	1	1
J_s [A/mm^2]	4.6	4.6	4.6	4.6	4.6
Excitation frequency, [Hz]	13.33	66.67	66.67	66.67	66.67
PM mass/% of total weight [kg]	11.3/3.6%	24.8/7.9%	25.2/8%	11.5/3.7%	11.9/3.8%
Torque [Nm]	534	384	605	912	946
Torque density (over total vol.) [Nm/L]	17.3	12.2	19.4	29.4	30.5
Power factor [lagging]	0.8	0.61	0.62	0.83	0.85
Stator OD [mm]	355.6	355.6	355.6	355.6	355.6
Stack length [mm]	311	311	311	311	311

IV. CONCLUSION

It has been demonstrated that a VM topology having q=1 and $P_r^{SVPM} = (6q-1)P_s$, the back-emf can be improved up to 3 times compared with an IPM and torque production can be proportionally increased by the same amount. Furthermore, an alternating flux barrier SVPM using ferrite PMs has been proposed, the FEA results suggest that, the proposed SVPM effectively improve the back-emf/torque production of a conventional SVPM, the torque production even surpasses that of a benchmark rare earth magnet assisted IPM under the same stator current density condition, with the tradeoff being that the magnet weight is increased while the power factor is lowered due to the use of ferrite magnets. Alternative topologies such as V-shape and U-shape topologies using rare earth magnets were also introduced, and given the same magnet usage, the V-/U-shape topology improved the torque by about 80%, and achieved a similar power factor compared with benchmark IPM machine. All of these three proposed topologies can be considered as a new family of VPMs which utilize alternating rotor leakage flux blocking effects. Overall, the simple structure and good torque capability make this new family of VPMs attractive and practical candidates for low-speed applications, such as industrial cooling fans, wind turbines, and marine propulsions

ACKNOWLEDGMENT

The authors express their gratitude to the companies of the Wisconsin Electric Machines and Power Electronics Consortium (WEMPEC) for assistance and support during this research.

REFERENCES

[1] C. H. Lee, "Vernier motor and its design," *IEEE Trans. Power Appar. Syst.*, vol. 82, no. 66, pp. 343–349, 1963.

[2] A. Ishizaki, T. Tanaka, K. Takahashi, and S. Nishikata, "Theory and Optimum Design of PM Vernier Motor." Electrical Machines and Drives Seventh International Conf., Durham, UK, 1995.

[3] A. Toba and T. A. Lipo, "Generic torque-maximizing design methodology of surface permanent-magnet vernier machine," *IEEE Trans. Ind. Appl.*, vol. 36, no. 6, pp. 1539–1546, 2000.

[4] B. Kim and T. A. Lipo, "Operation and Design Principles of a PM Vernier Motor," *IEEE Trans. Ind. Appl.*, vol. 50, no. 6, pp. 3656–3663, Nov. 2014.

[5] L. Wu, R. Qu, D. Li, and Y. Gao, "Influence of Pole Ratio and Winding Pole Numbers on Performance and Optimal Design Parameters of Surface Permanent-Magnet Vernier Machines," *IEEE Trans. Ind. Appl.*, vol. 51, no. 5, pp. 3707–3715, Sep. 2015.

[6] B. Kim and T. A. Lipo, "Analysis of a PM Vernier Motor With Spoke Structure," *IEEE Trans. Ind. Appl.*, vol. 52, no. 1, pp. 217–225, Jan. 2016.

[7] Z. S. Du and T. A. Lipo, "High torque density ferrite permanent magnet vernier motor analysis and design with demagnetization consideration," in *Energy Conversion Congress and Exposition (ECCE), 2015 IEEE*, 2015, pp. 6082–6089.

[8] B. Heller and V. Hamata, *Harmonic Field Effects in Induction Machines*. Amsterdam, The Netherlands: Elsevier, 1977.

[9] T. A. Lipo, *Introduction to AC Machine Design*, 3rd ed. Madison, WI: Wisconsin Power Electronics Research Center, 2016.

[10] X. Ge, Z. Q. Zhu, J. Li, and J. Chen, "A Spoke-Type IPM Machine With Novel Alternate Airspace Barriers and Reduction of Unipolar Leakage Flux by Step-Staggered Rotor," *IEEE Trans. Ind. Appl.*, vol. 52, no. 6, pp. 4789–4797, Nov. 2016.